IEEE Access
Multidisciplinary ⋮ Rapid Review ⋮ Open Access Journal

Received January 17, 2021, accepted February 11, 2021, date of publication February 18, 2021, date of current version March 2, 2021.

Digital Object Identifier 10.1109/ACCESS.2021.3060017

The Optimal Current Ratio Control of Redundant Electric Drive Systems and Diagnostic Strategies for Disagreement

YOUNGWOO NOH, WONKYU KIM, AND JU LEE, (Senior Member, IEEE)
Department of Electrical Engineering, Hanyang University, Seoul 04763, South Korea
Corresponding author: Ju Lee (julee@hanyang.ac.kr)

ABSTRACT As research into technology for autonomous vehicles becomes ever more intensive, the need for redundant system designs, as a solution for fail-operational functionality, has also increased. Redundant systems are those involved in maintaining normal operation even when one or more components fails. In particular, in electric power steering (EPS) systems, redundancy is achieved by applying dual-winding (DW), permanent magnet synchronous motors (PMSMs) and dual electronic control units (ECUs). In this study, the torque and efficiency of DW-PMSMs is analysed based on the manner in which the currents in each winding mechanism are combined. It was found that the PMSMs have maximum torque and efficiency when the current ratio was the same between DWs. A diagnostic strategy is proposed whereby the phase current ratio of dual lanes is not matched. The proposed diagnostic process includes the selection of the optimal fault threshold of the current difference between two ECUs and a method for distinguishing which of these was a failure for disagreement. In addition, depending on whether or not failure detection has occurred, a current compensation control method is proposed for reverting to normal operation or for failure operations. The dual-lane system was fabricated and the proposed solutions were experimentally verified.

INDEX TERMS Automotive redundant systems, dual three-phase permanent magnet synchronous motors, dual electronic control units, current ratio, optimal fault threshold, diagnosis, disagreement, fail-operational system, current compensation control, functional safety.

I. INTRODUCTION

Owing to the commercialisation of autonomous vehicles, there is increasing demand for passenger safety. It is becoming difficult to create functional safety designs under such circumstances given the highly rigorous requirements of ISO26262, the functional safety standard specification for automotive components [1], [2]. In light of the fact that failures of electrical automotive components in autonomous vehicles can lead to fatal accidents, solutions are being explored to ensure continuous operation, even in the event of an electrical fault. In previous electric power steering (EPS) systems, if an electrical fault occurred in a motor or an electronic control unit (ECU), the safe state, also called the ''fail-safe'' or ''fail-silence'', targeted error detection and reaction. In other words, existing systems pursue ''no torque assist'' as a safe state. In autonomous driving systems, however, the safe state of a fail-operational system should target error detection, isolation, and failure recovery. Stated differently, the safe state of the EPS system changes from ''no torque assist'' to ''permanent torque assist''. In order to satisfy this safe state, redundant design is one of the solutions currently being explored.

Redundant systems facilitate a fail-operational function in which one side fails and the other maintains normal operations. Redundant design concepts that can adequately isolate the faulty part and maintain functional operation with alternative hardware are being widely investigated as solutions to fail-operational systems [3]–[5]. Typically, in such redundant systems, dual three-phase motors are employed and dual ECUs are designed as two electrically-isolated units [6]–[9]. As is shown in Fig. 1(a), a steer-by-wire EPS system, defined in SAE for level 4 and 5 autonomous vehicles, has a redundant system configuration with two battery voltage supply lines. This configuration consists of dual-winding (DW) motors and dual ECUs, and each lane has a separate battery voltage

The associate editor coordinating the review of this manuscript and approving it for publication was Wei Xu.

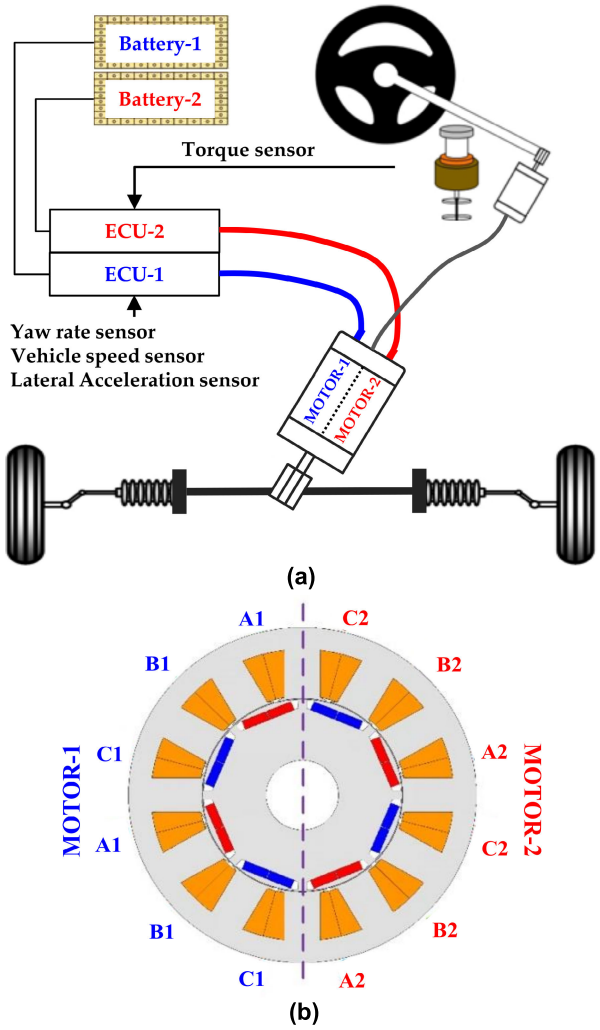

FIGURE 1. Structure of redundant systems: (a) mechanical structure of a steer-by-wire EPS system, (b) DW structure of PMSMs.

supply line and ground. Fig. 1(b) shows the DW structure of the permanent magnet synchronous motors (PMSMs) used in the dual lanes. Windings −1 and −2 of the motors are symmetrically mounted at an angle of 180° with respect to one another. The electrical connections of windings −1 and −2 are independent, and their neutral points are separate.

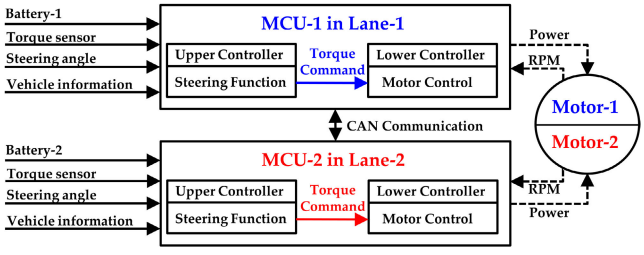

FIGURE 2. Functional block diagram of dual lanes.

Fig. 2 shows a functional block diagram of the dual-lane redundant systems. The micro-controller unit (MCU) of each lane is divided into two segments; an upper controller that calculates the steering function and a lower one that controls the motor. The steering function component calculates the torque command for the motor control by means of torque sensing values, steering angle and vehicle information from an external interface. The motor control component supplies power to the motor in accordance with the calculated torque command. For normal operation, each lane produces up to a maximum of 50% of the output, which means the sum of maximum outputs of the two lanes totals 100%. When the DW-PMSMs generate the maximum torque (100%), 50% of the total required current flows into each separate winding. If a fault occurs in one lane, the faulty lane is disabled and isolated, with the normal lane operated with up to 50% of the total output power at maximum. In EPS systems, it is possible to achieve the steering assist function at high speeds, even with a torque output of less than 50%.

However, if the total output required is 50% instead of 100%, the output ratios of each lane can vary from a performance viewpoint, such as 25%:25%, >25%: <25%, or vice versa. For instance, if the maximum output of each lane is 2.5 Nm, the maximum output of each redundant system is 5 Nm. For realising the maximum output, each lane output should be 2.5 Nm. However, if the target torque command is 2.7 Nm, the redundant system should choose whether to equally output 1.35 Nm from each lane or to output the torque with different ratios, such as 1.7 Nm:1.0 Nm. It is necessary to investigate the optimal current ratios of each winding from the viewpoint of achieving the maximum torque performance or the maximum efficiency of the DW-PMSMs.

After the proper current ratio has been determined in terms maximising performance, if the current ratio is not controlled as intended, there is a problem in determining whether this is caused by a hardware deviation or malfunction of the MCU between the two lanes. If it is not a fault or damage of the components, but a deviation between the two lanes such as with respect to current sensing, a control compensation method is needed to return to normal current ratio as intended in order to achieve optimal performance. If there is a malfunction of the MCU, such as an incorrect torque command or current calculation error, in order to satisfy the safety goal, the failed lane must be isolated and the torque assist operation maintained using another normal lane. Short-circuits or damage to semiconductor devices can be detected by means of well-known diagnostic method and the MCU for automotive safety integrity level (ASIL) includes one or more lock-step cores, and so hardware failures of the MCU can be easily detected. However, if the two MCUs calculate differently, such as due to computational errors rather than hardware failures, the problem arises of distinguishing which of the dual lanes is true or false.

In this study, we theoretically analyse and derive the optimal current ratio in light of the maximum torque performance and efficiency of the DW-PMSMs. And when the redundant systems could not be controlled in accordance with the intended current ratio, we propose an optimal diagnostic threshold that can distinguish true and false faults and propose

a fault judgment method to distinguish which MCU undergoes a failure between the dual lanes. Moreover, a current compensation control strategy for normal operation recovery and failure operation is proposed.

II. CALCULATION OF DW-PMSMS TORQUE AND EFFICIENCY USING CURRENT RATIOS

In order to estimate the torque performance of the system, it is necessary to investigate the inductance of DW-PMSMs according to their current ratios. To analyse the inductance of the DW-PMSMs, the inductance of each motor should be obtained as a function of the phase current magnitude. With ECU-1 turned on and ECU-2 turned off, the inductance of motor-1 can be calculated from the voltage equation of the d-axis while increasing the q-axis current from 0 A to 70 A through winding-1:

$$V_{dk} = R_a i_{dk} + L_{dk}\frac{d}{dt}i_{dk} - \omega_r L_{qk} i_{qk}, \quad (k = 1, 2) \tag{1}$$

where R_a is the stator winding resistance, i_{dk} and i_{qk} are the dq-axes currents, respectively, L_{dk} and L_{qk} are the dq-axes inductance, ω_r is a synchronous angular speed, and the subscripts k denote motors -1 and -2. With the DW-PMSMs shown in Fig. 1(b), the d-axis was controlled with zero current ($i_{d1} = 0$ A), and the values of V_{d1} were experimentally measured as the magnitude of i_{q1} was increased and the measured V_{d1} were negative values. The electrical speed was 1000 rpm, which means that ω_r was fixed. With the measured V_{d1} and i_{q1}, the value of L_{q1} could be calculated by means of equation (2):

$$L_{q1} = -\frac{V_{d1}}{\omega_r i_{q1}} \tag{2}$$

The inductance of motor-2 could be calculated in the same way as that of motor-1; that is, with ECU-1 turned off and ECU-2 turned on. The changes in L_{q1} and L_{q2} as the q-axis currents increased from 0 A to 70 A are shown in Fig. 3(a). When $i_{qk} = 0$ A, the L_{qk} was estimated using the interpolation method with the inductance values calculated from 7–70 A of i_{qk}. It can be known that the values of L_{q1} and L_{q2} decreased as the q-axis currents increased. In this instance, the sum of the total inductance ($L_{sum} = L_{q1} + L_{q2}$) of the DW motors is shown Fig. 3(b). The value of L_{sum} is the highest when the current ratios are equal and the value decrease as the difference between the current ratios increases.

If the battery input voltages and rotor position sensing values of ECUs -1 and -2 are the same, the PMSMs with the concentrated symmetrically-mounted windings of 8-pole and 12-slot combination have very little mutual inductance effects on the torque output. The sum of the torque outputs when driving motors -1 and -2 separately and the torque output of the DW motors is then matched. Therefore, the consideration of the mutual electromagnetic coupling was excluded.

Considering the change in inductance according to the difference between the currents through each of the windings, it was possible to estimate the change in torque. The sum of the total torque and the torque of each motor could be computed using equations (3) and (4), respectively [10]. At the rotation speed of 1000 rpm, the d-axis was under zero-current control, but a very small current actually flowed, and so we assumed $i_{dk} = -0.1$ A for the torque calculation. Experimentally, the d-axis inductance L_{dk} barely changed, and the change in the magnetic flux linkage ϕ_{fk} was marginal depending on the difference between the q-axis currents of each of the windings. Here the L_{dk} was assumed to be fixed. Therefore, by using equations (3) and (4), the change in torque according to ϕ_{fk}, L_{qk} and i_{qk} could be calculated:

$$T_{sum} = T_1 + T_2 \tag{3}$$

$$T_k = P_n\left(\phi_{fk} i_{qk} + \left(L_{dk} - L_{qk}\right) i_{dk} i_{qk}\right), \quad (k = 1, 2) \tag{4}$$

where P_n is the number of pole pairs.

Fig. 3(c) shows that the combined torque T_{sum} is highest when the current ratios are equal, whereas the torque decreases as the difference between the current ratios increases. The graph of the torque change is very similar to that of the inductance change. However, the magnitude of change in torque with the difference between the two motor currents is very small because the value of the inductance itself is small, even when the inductance changes. Although the magnitude of the torque change owing to the current difference is small, the torque changes as the current difference does under the same conditions.

Fig. 3(d) shows the change in the total loss of the DW-PMSMs as the q-axis currents change from 0 A to 70 A. In order to calculate the efficiency of the DW-PMSMs, it was necessary to calculate their total loss as the current ratios changed. The copper loss of the DW-PMSMs $W_{c\ sum}$ could be computed using equations (5)–(7). Because the d-axis current was zero-current controlled, equations (5) and (6) can be expressed as functions of the stator winding resistance and the current flowing through each motor, as in equation (7):

$$W_{ck} = R_a\left(i_{dk}^2 + i_{qk}^2\right), \quad (k = 1, 2) \tag{5}$$

$$W_{c\ sum} = W_{c1} + W_{c2}, \quad (i_{d1},\ i_{d2} = 0A) \tag{6}$$

$$W_{c\ sum} = R_a\left(i_{q1}^2 + i_{q2}^2\right) \tag{7}$$

According to equation (7), $W_{c\ sum}$ increases as the difference between i_{q1} and i_{q2} does. The iron loss of the DW-PMSMs $W_{i\ sum}$ relates to the eddy current and the hysteresis loss of the core owing to temporal variation in the magnetic fields [11].

The change in iron loss according to the current ratios of the windings was compared via simulation. In this simulation, the motor rotation speed was fixed to 1000 rpm. The simulation results indicate that the iron loss increased to a greater extent when the current ratios changed than when the current ratios were constant, as is shown in Fig. 4(a) and (b). When the currents between the windings were equal, as in Fig. 4(a), $W_{i\ sum} = 2.77$ W, and when the difference between the winding currents was the maximum, as in Fig. 4(b), $W_{i\ sum} = 3.25$ W. This can be attributed to the fact that the core loss

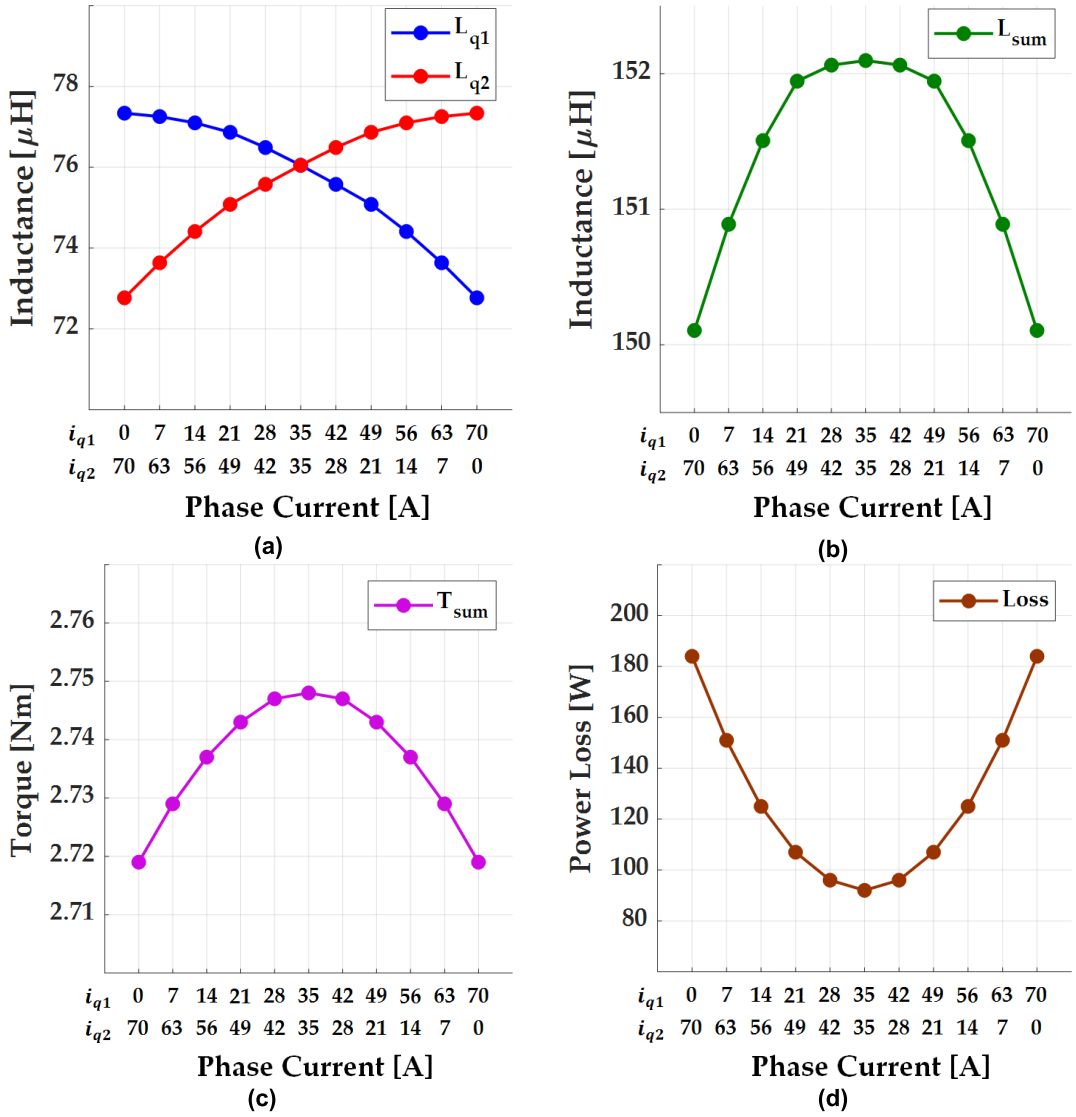

FIGURE 3. According to the phase current ratios: (a) change in the inductance of each motor, (b) change in the inductance of the DW-PMSMs, (c) change in the torque of the DW-PMSMs, (d) change in power loss of the DW-PMSMs. The horizontal axis represents the different q-axis currents in each motor. The sum of i_{q1} and i_{q2} is 70 A.

increases as the magnetic flux density B_m does, as in equation (8):

$$P_{core\ loss} = k_h f B_m^2 + k_e f^2 B_m^2 \tag{8}$$

where k_h is the hysteresis loss coefficient, k_e is the eddy current loss coefficient, and f is the switching frequency. Compared to the output power of the DW motors, the iron loss and its changes are very small depending on the ratios of the currents flowing through each winding. The total loss of the DW-PMSMs is mostly copper loss. The efficiency of the DW-PMSMs, η is expressed by equation (9):

$$\eta = \frac{T_{sum}\omega_r / P_n}{T_{sum}\omega_r / P_n + W_{c\ sum} + W_{i\ sum}} \tag{9}$$

The larger the difference between the currents flowing through each of the windings, the larger the copper loss $W_{c\ sum}$ and the magnitude of change in T_{sum} is smaller than that of the change in the loss. Therefore, the efficiency of the DW-PMSMs is the highest when the current ratios are equal, and the motor efficiency decreases as the difference between the currents increases. In summary, considering the torque and efficiency of the DW-PMSMs, the current ratios of each winding should be equal in order to achieve optimal performance. Therefore, it is necessary to ensure that the ratios of the currents flowing through each winding are always equal in the normal status.

III. PROPOSAL FOR AN OPTIMAL FAULT THRESHOLD AND FAULT JUDGMENT METHOD

A problem in which one of two lanes does not operate due to a failure of hardware can be easily diagnosed, but if both lanes operate but there is disagreement between the two lanes, it is

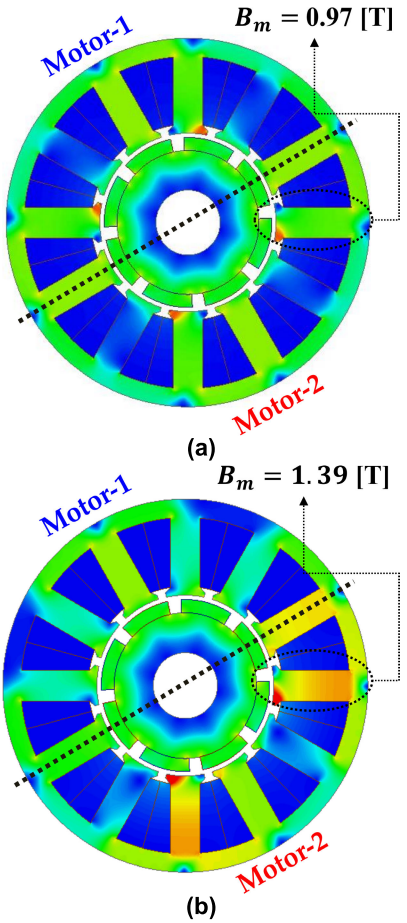

FIGURE 4. Simulation result of the iron loss according to the current difference between motors −1 and −2: (a) $i_{q1} = 35$ A: $i_{q2} = 35$ A, (b) $i_{q1} = 0$ A: $i_{q2} = 70$ A.

necessary to analyse how best to diagnose it. As previously determined, the current ratios in the dual lanes should be the same, but if there is a difference, it is necessary to first determine how much the current difference should occur to be considered a fault, and secondly, which of the two lanes is faulty. In order to solve the problem of how much more of a current difference will be found to be a failure, it is important to distinguish whether a current difference occurs due to an inevitable deviation, such as a dispersion error in electronic components and calculations related to current sensing, or whether it is due to an incorrect torque command calculation by the MCU. As the suitable reaction depends on whether or not it is a failure, an accurate diagnosis is required, as is the selection of an optimal fault threshold to confirm a failure. The diagnostic threshold is defined as the difference in phase currents between the two lanes, $\boldsymbol{\varepsilon}$.

If the torque command values of the two MCUs are equal and the current difference between the two lanes occurs below $\boldsymbol{\varepsilon}$, it can be considered a deviation in each lane rather than a failure. It is necessary to recover the currents between the two lanes equally by again controlling the currents. In other words, it is necessary to retry the diagnosis prior to detecting it as a failure and entering the safe state. If the current difference is below $\boldsymbol{\varepsilon}$ but the torque command values of the two MCUs differ, and if the current difference occurs above $\boldsymbol{\varepsilon}$, they can be considered a failure, not a deviation, and after identifying which MCU has failed, the faulty lane enters the safe state so as to not violate the safety goals.

What should be considered along with the fault threshold in the diagnosis is the filtering time for confirming the failure. This is also called the qualification time, and it can be set as a counter base or time base. The qualification time for detecting an intrinsic fault in order to prevent a false fault due to temporary errors or system noise is defined as t_{qt}. In other words, the current difference between the two lanes is confirmed as a failure after at least t_{qt} time has elapsed. The timespan from the detection of a fault to a reaction to it, including t_{qt}, constitutes the fault-tolerant time interval, which in this study was assumed to be 100 ms.

A. CALCULATION AND SELECTION OF THE OPTIMAL FAULT THRESHOLD

In order to determine the fault threshold $\boldsymbol{\varepsilon}$, the current-sensing deviation, which comprises a direct cause of the current difference, should be considered. In the EPS ECU, instead of the hall sensor type, a shunt resistor has typically been used recently as a current sensor to reduce the design cost. When the motor current flows, the voltage at both ends of the shunt resistor is sensed and amplified by the current sense amplifier and then the analogue voltage is sensed by the analogue digital converter (ADC) channels of the MCU. The $\boldsymbol{\varepsilon}$ can be calculated by considering the deviations from the shunt resistor, current sense amplifier and ADC module of the MCU. Fig. 5 shows a simplified circuit diagram of the entire current-sensing hardware path.

When a positive and negative phase current flows through the shunt resistor, the voltage across the resistor enters the input of the current sense amplifier. This differential input voltage V_{id} is expressed in equation (10). The shunt resistance had a maximum deviation of 1.75% when the tolerance of the resistance and temperature coefficient were considered. V_{id} has minimum and maximum values according to the deviation in the shunt resistance. The current sense amplifier in Fig. 5 featured a gain $A_v = 10$ and the output offset zero-point voltage $V_{of} = 2.5$ V. The minimum and maximum values of the voltage output of the current sense amplifier V_o are expressed by equation (11), considering the input offset error V_{if}, gain error A_{ve} and output offset error V_{ofe}. The output voltage V_o is inputted into the ADC channels of the MCU and converted into a digital value, V_{o_ADC}. In the process of converting V_o to V_{o_ADC}, it is expressed as equation (12) because the ADC module also features the following errors. As the ADC module is supplied with a separate analogue voltage from the external regulator, there is an output voltage tolerance of the regulator V_{ADC_R}. There is also an ADC error voltage V_{ADC_E} such as RMS noise or input-referred noise. Converting the V_{o_ADC} to a phase current value with V_{of}, A_v and R_S renders it the finally sensed phase current

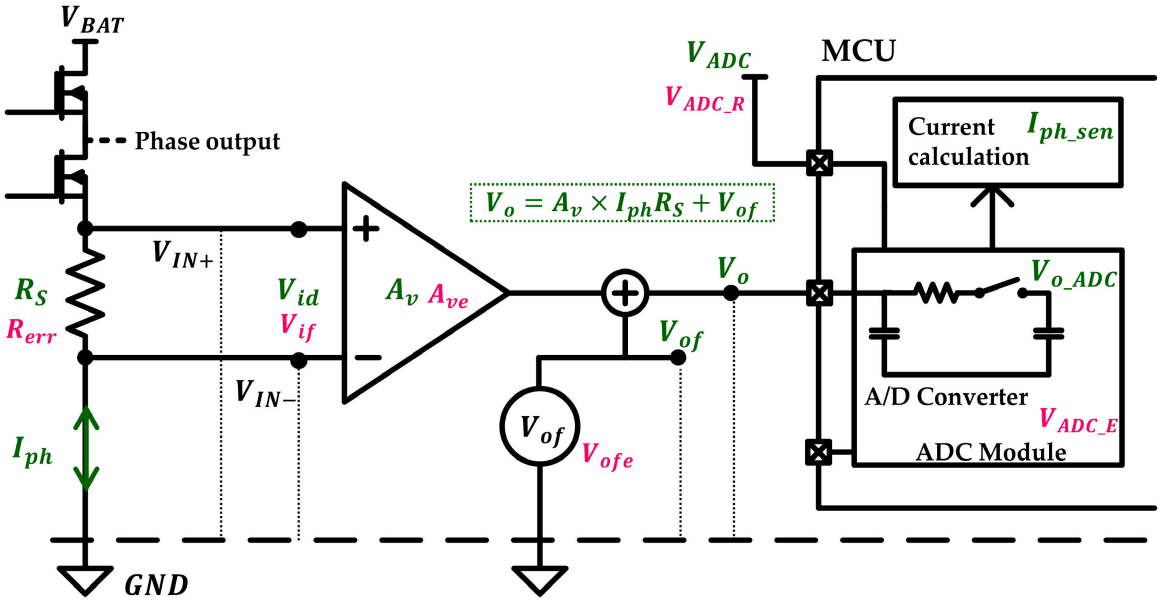

FIGURE 5. Simplified circuit diagram of the current-sensing hardware path.

TABLE 1. Current-sensing-related parameters and worst-case analysis results.

Item		Parameters	Unit	Minimum value	Typical value	Maximum value	Comments
Phase current		I_{ph}	A	−70		70	
Shunt Resistor	Total error rate of resistance	R_{err}	%	−1.75		1.75	
	Resistance considering error	R_S	mΩ	1.965	2.000	2.035	
Current sense amplifier	Differential input voltage	V_{id}	V	0.138	0.140	0.142	When I_{ph}=70 A, it was calculated by equation (10).
	Input offset voltage	V_{if}	mV	−1		1	
	Output offset	V_{of}	V		2.5		
	Output offset error	V_{ofe}	mV	−50		50	
	Gain	A_v	-		10		
	Gain error	A_{ve}	-	0.99		1.01	Error rate : ±1%
	Amplifier output voltage	V_o	V	3.801	3.900	3.998	When I_{ph}=70 A, it was calculated by equation (11).
MCU	ADC reference voltage tolerance	V_{ADC_R}	-	0.99		1.01	Tolerance rate : ±1%
	ADC error voltage	V_{ADC_E}	mV	−1.1		1.1	
Output voltage converted to ADC		V_{o_ADC}	V	3.762		4.039	When I_{ph}=70 A, it was calculated by equation (12).
Finally sensed phase current value corresponding to V_{o_ADC} value		I_{ph_sen} [a]	A	63.13	70	76.99	When I_{ph}=70 A

[a]When converting from V_{o_ADC} to I_{ph_sen}, the formula is as follows: $I_{ph\_sen} = \frac{V_{o\_ADC} - V_{of}}{A_v \times R_S(Typ.)}$

value I_{ph_sen}. All of the values of the parameters that can affect the current-sensing deviation and the worst-case analysis process using the minimum-maximum method are shown in Table 1.

$$V_{id} = V_{IN+} - V_{IN-} = I_{ph} \times R_S \quad (10)$$

$$V_o = (V_{id} + V_{if}) \times (A_v \times A_{ve}) + (V_{of} + V_{ofe}) \quad (11)$$

$$V_{o\_ADC} = (V_o \times V_{ADC\_R}) + V_{ADC\_E} \quad (12)$$

In the worst case, the converted sensing current I_{ph_sen} can have a current deviation of ±7 A. The 7 A is the deviation of the current that can occur in one lane, and so the deviation of the current difference that can occur in two lanes is a maximum of 14 A in the worst case. Under normal status, the difference in the current that can be caused by deviations between the two lanes cannot exceed 14 A. Therefore, $\boldsymbol{\varepsilon}$ was selected as 14 A.

If the torque command values are the same and the difference in the current is less than 14 A, it should first be

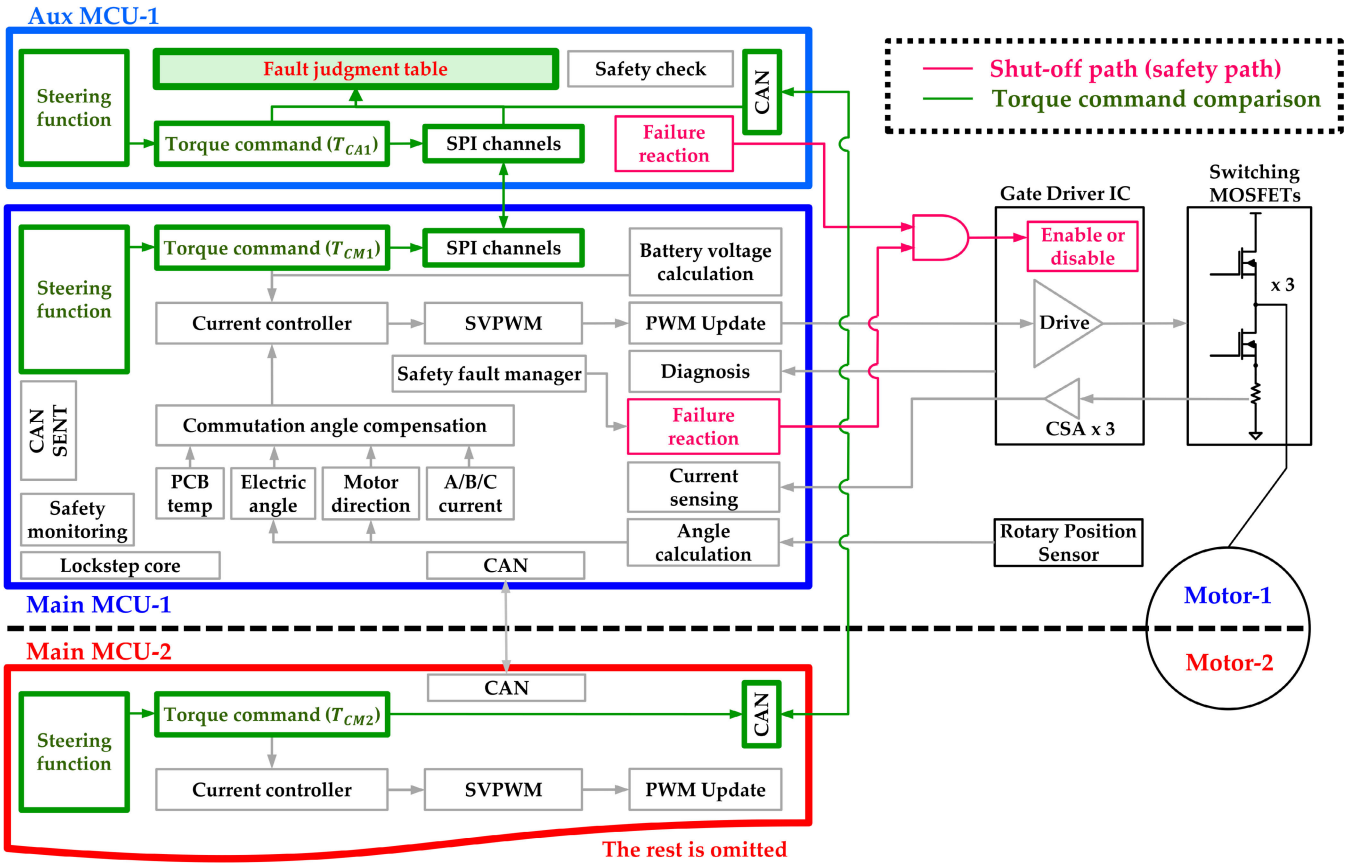

FIGURE 6. Proposal of an interdependent monitoring system between dual lanes using an aux MCU.

considered that the current mismatch is not due to a fault in the MCU, but to a deviation in current-sensing. In other words, an attempt must be made to again equalise the currents of the dual lanes through the current control before it is judged to be a failure. However, if the current difference is greater than 14 A, either lane is considered to have failed. An optimal diagnostic threshold $\boldsymbol{\varepsilon}$ was derived through the worst-case analysis of current-sensing deviation.

B. PROPOSAL OF THE FAULT JUDGMENT TABLE FOR DISAGREEMENT BETWEEN THE DUAL LANES

The phase current of each lane varies according to the torque command T_{CM1} and T_{CM2} calculated by the steering function module of each MCU. Typically, electronic component damage such as battery or ground to short-circuit or chip defects can be easily detected through diagnostic functions, but it is difficult to detect MCU calculation errors such as the algorithm edge error, memory error or overflow. An abnormal calculation of the MCU due to software errors leads to an incorrect torque command and outputs a false phase current.

If the current difference between the two lanes is less than $\boldsymbol{\varepsilon}$, and the T_{CM1} and T_{CM2} values are the same, it can be recognised as a current deviation due to the current-sensing deviation as described above. However, if the current difference between the two lanes is greater than $\boldsymbol{\varepsilon}$ or the T_{CM1} and T_{CM2} values differ, it is necessary to distinguish which MCU operation is true. If the triple-redundancy concept is applied to the failure operation, the same algorithm is executed in three identical cases, and these calculated values or phase currents are compared to each other and the failed MCU can be identified as a majority decision principle (two are the same and one is different). However, in the automotive EPS application, the architecture of the dual-redundant design concept is primarily used due to the complexity and cost of the hardware. In such a dual-redundant system, there can be disagreement between T_{CM1} and T_{CM2}, leading to a situation called a "byzantine-fault".

In order to distinguish which of the two MCU operations was true in the dual-redundant system, an interdependent monitoring system is proposed, as is shown in Fig. 6. In general, in EPS systems that must meet ASIL-D, a multi-core MCU is primarily used and so there is a separate core that can monitor other processors while simultaneously performing the same algorithm or calculation. In this study, in addition to the primary single-core MCU with lock-step core (main MCU) that directly controls the PMSM, a separate additional auxiliary monitoring MCU (aux MCU) was applied place of the multi-core MCU. The aux MCU in each lane received the same battery supply and external signals, such as torque sensing values and steering angle values, and also calculated the torque command value using the same algorithm as the

TABLE 2. Fault judgment table for a single-point fault.

Component	Main MCU-1	Aux MCU-1	Main MCU-2	Aux MCU-2	Reaction
Torque Command	T_{CM1}	T_{CA1}	T_{CM2}	T_{CA2}	
Comparison	-	$(T_{CM1}, T_{CA1}, T_{CM2})$	-	$(T_{CM2}, T_{CA2}, T_{CM1})$	
Judgment	-	Normal or Fail	-	Normal or Fail	
Case 1	A [a] - -	B (A, B, B) T_{CM1} failed	B - -	B (B, B, A) T_{CM1} failed	The main MCU-1 has a fault. Therefore, shut off lane-1.
Case 2	B - -	A (B, A, B) T_{CA1} failed	B - -	B (B, B, B) Normal	T_{CM1} and T_{CM2} are normal. No current difference. Therefore, case 2 can be excluded.
Case 3	B - -	B (B, B, A) T_{CM2} failed	A - -	B (A, B, B) T_{CM2} failed	The main MCU-2 has a fault. Therefore, shut off lane-2.
Case 4	B - -	B (B, B, B) Normal	B - -	A (B, A, B) T_{CA2} failed	T_{CM1} and T_{CM2} are normal. No current difference. Therefore, case 4 can be excluded.

[a]A and B are the calculated torque command values of each MCU.

TABLE 3. Fault judgment table for a dual-point fault.

Component	Main MCU-1	Aux MCU-1	Main MCU-2	Aux MCU-2	Reaction
Torque Command	T_{CM1}	T_{CA1}	T_{CM2}	T_{CA2}	
Comparison	-	$(T_{CM1}, T_{CA1}, T_{CM2})$	-	$(T_{CM2}, T_{CA2}, T_{CM1})$	
Judgment	-	Normal or Fail	-	Normal or Fail	
Case 5	A [a] - -	B (A, B, C) Be shelved	C - -	C (C, C, A) T_{CM1} failed	The main MCU-1 has a fault. Therefore, shut off lane-1.
Case 6	A - -	C (A, C, B) Be shelved	B - -	C (B, C, A) Be shelved	It is impossible to judge. Therefore case 6 was excluded.
Case 7	A - -	C (A, C, C) T_{CM1} failed	C - -	B (C, B, A) Be shelved	The main MCU-1 has a fault. Therefore, shut off lane-1.
Case 8	C - -	A (C, A, B) Be shelved	B - -	C (B, C, C) T_{CM2} failed	The main MCU-2 has a fault. Therefore, shut off lane-2.
Case 9	C - -	A (C, A, C) T_{CA1} failed	C - -	B (C, B, C) T_{CA2} failed	T_{CM1} and T_{CM2} are normal. No current difference. Therefore, case 9 can be excluded.
Case 10	C - -	C (C, C, A) T_{CM2} failed	A - -	B (A, B, C) Be shelved	The main MCU-2 has a fault. Therefore, shut off lane-2.

[a]A, B, and C are the calculated torque command values of each MCU.

main MCU. The aux MCU monitors the main MCU in the same lane through SPI communication, because they thereby have the same power and ground, and monitors the main MCU in the other lane through CAN communication because they have different power and ground settings separated. Therefore, the aux MCU in lane-1 can compare its own calculated torque command value T_{CA1}, T_{CM1} of the main MCU-1 in the same lane, and T_{CM2} of the main MCU-2 in the other lane. The aux MCU in lane-2 can also compare T_{CA2}, T_{CM2}, and T_{CM1}. Each aux MCU compares the three calculated torque command values with each other, and if all three values are the same, it determines as normal, and if the two values are the same and one is different, it determines that the MCU with different values is abnormal.

Using the proposed interdependent monitoring system, the proposed fault judgment tables for disagreement in all cases between the dual lanes are described in Tables 2 and 3. Table 2 shows that, in the case of a single-point fault, each aux MCU compares the calculated torque command values and can easily identify the faulty MCU by means of the majority decision principle. And which reactions are appropriate in each case was also defined. Cases 1 and 3 shut off the lane with the faulty main MCU, and continue the torque assist operation with the other normal main MCU.

As for the torque assist in such a fail-operational situation, a limited torque assist can be provided because one lane was inoperable. Cases 2 and 4 were not the main MCU failure, but the aux MCU failure, and so the reaction was expected for maintaining the current operation. As the aux MCUs were not involved in the motor control, the same motor current flows through each winding. Therefore, cases 2 and 4 can be excluded from the proposed fault judgment table, because T_{CM1} and T_{CM2} were the same and so there is no current difference.

In the functional safety analysis of the ASIL-D system, not only the single-point fault but also dual-point fault must be analysed. Table 3 shows the case of a dual-point fault. Cases 5, 7, 8 and 10, given that either MCU-1 or MCU-2 are a failure, shut off the failed lane and maintained the failure operation within the normal lane. For instance, in case 5, the aux MCU-1 maintains the determination of the failure because all three calculated torque command values differed, but aux MCU-2 can determine the main MCU-1 to be a failure because only T_{CM1} has a different value. In the reaction of case 5, lane-1 is shut off and the failure operation performed with lane-2. Cases 7, 8 and 10 are the same as in case 5.

However, in case 6, it can be judged that both MCUs -1 and -2 are a failure, and so it must be decided how the reaction should be performed. In such a case, the fail-operational safety goal can be violated if both lanes are shut off. The reaction for case 6 can vary according to vehicle type, the claimed failure rate in the evaluation of the probability of the violation of safety goals, and the steering scenario for a crisis situation. This is a very rare special case and an emergency reaction must be derived. This reaction is being handled in carmaker or automobile industry according to emergency driving scenario. Case 6 is very unlikely to occur in functional safety situations. For instance, if the failure rate of one MCU is 5 fit, the failure rate due to the simultaneous faults of the MCUs in both lanes can be calculated as a 25×10^{-9} fit. In this study, case 6 was excluded. This is because the probability of occurrence was extremely low, and even if a scenario such as case 6 occurs, the failure rate of 10 fit or less, which is the requirement of ASIL-D, can be satisfied. In conclusion, the proposed fault judgment table can be used as a tool to solve the ''tie-breaking'' situation; that is, to determine which MCU has a fault.

IV. PROPOSAL OF THE CURRENT DIFFERENCE MANAGEMENT METHOD AND DUAL THREE-PHASE CURRENT COMPENSATION CONTROL METHOD

Using the fault threshold value of the current difference between the two lanes and the fault judgment table proposed in the previous section, a current difference management method (CDMM) is proposed. The CDMM offers a comprehensive solution for distinguishing between a non-failure and failure, and how to detect and react in the case of a failure. A current compensation control method (CCCM) was also proposed, which is a solution for removing the current difference between the dual lanes and increasing the current of the normal lane to perform a failure operation. The overall flow chart of the CDMM and proposed CCCM are shown in Fig. 7.

A detailed description of the flowchart of the CDMM is as follows:

1) Each phase current, I_{ak}, I_{bk} and I_{ck}, $(k = 1, 2)$, is sensed by the shunt resistor of each ECU and the average of the maximum phase currents, I_{ph_max1} and I_{ph_max2}, are compared to each other. The difference between I_{ph_max1} and I_{ph_max2} is defined as I_{ph_comp}.
2) If the maximum phase current values of each of the ECUs are equal ($|I_{ph\_comp}| = 0$), the previous PWM output is maintained. If there is a difference ($|I_{ph\_comp}| > 0$) over t_{qt} time, it is determined whether the difference is greater or less than the fault threshold $\boldsymbol{\varepsilon}$.
3) If $|I_{ph\_comp}|$ is greater than $\boldsymbol{\varepsilon}$, it is determined that a current difference occurred due to a malfunction of the MCU, and this is entered into the fault judgment table. If $|I_{ph\_comp}|$ is less than $\boldsymbol{\varepsilon}$, it should be determined whether there is a difference between T_{CM1} and T_{CM2}.
4) If T_{CM1} and T_{CM2} are not equal, it is assumed that there is also a malfunction in the MCU and this is entered into the fault judgment table. If T_{CM1} and T_{CM2} are equal, the main MCUs have no fault and the torque commands are correctly calculated. The difference in current occurs due to a deviation in each lane and the proposed CCCM shall be applied to each of them.
5) In the CCCM, the proportional current gain, P_k, $(k = 1, 2)$, is defined as the ratio of the calculated current values corresponding to the torque command value of each MCU that was previously verified, $I_{T_{CMk.cal}}$, $(k = 1, 2)$ and the sensed peak phase current values of each ECU, I_{pk_Peak}, $(p = a, b, c, k = 1, 2)$. Each phase current shall be compensated by P_k and the current difference shall disappear.
6) Finally, the PWM output of the gate driver ICs is changed so that the same current flows through each winding.
7) On the other hand, regardless of whether the difference in current is larger or smaller than $\boldsymbol{\varepsilon}$, if it is determined that the MCU has a fault, the MCU that has a fault is identified through the fault judgment table.
8) If the main MCU-1 or -2 is determined to have a failure, the shut-off path of the failed MCU is taken and the corresponding motor operation stopped.
9) The other normal lane increases the phase current by applying the proposed CCCM in order to provide the necessary output for the torque assist in the failure operation. The maximum output of one lane is 50% of the maximum output T_{max} of the dual lanes.
10) If the target torque command T_{tgt} that the dual lanes must output for the normal torque assist is less than half of the T_{max} of the dual lanes, the proportional current gain, P_{k*}, $(k = 1, 2)$, of the normal lane is adjusted by the calculated magnitude of the current corresponding

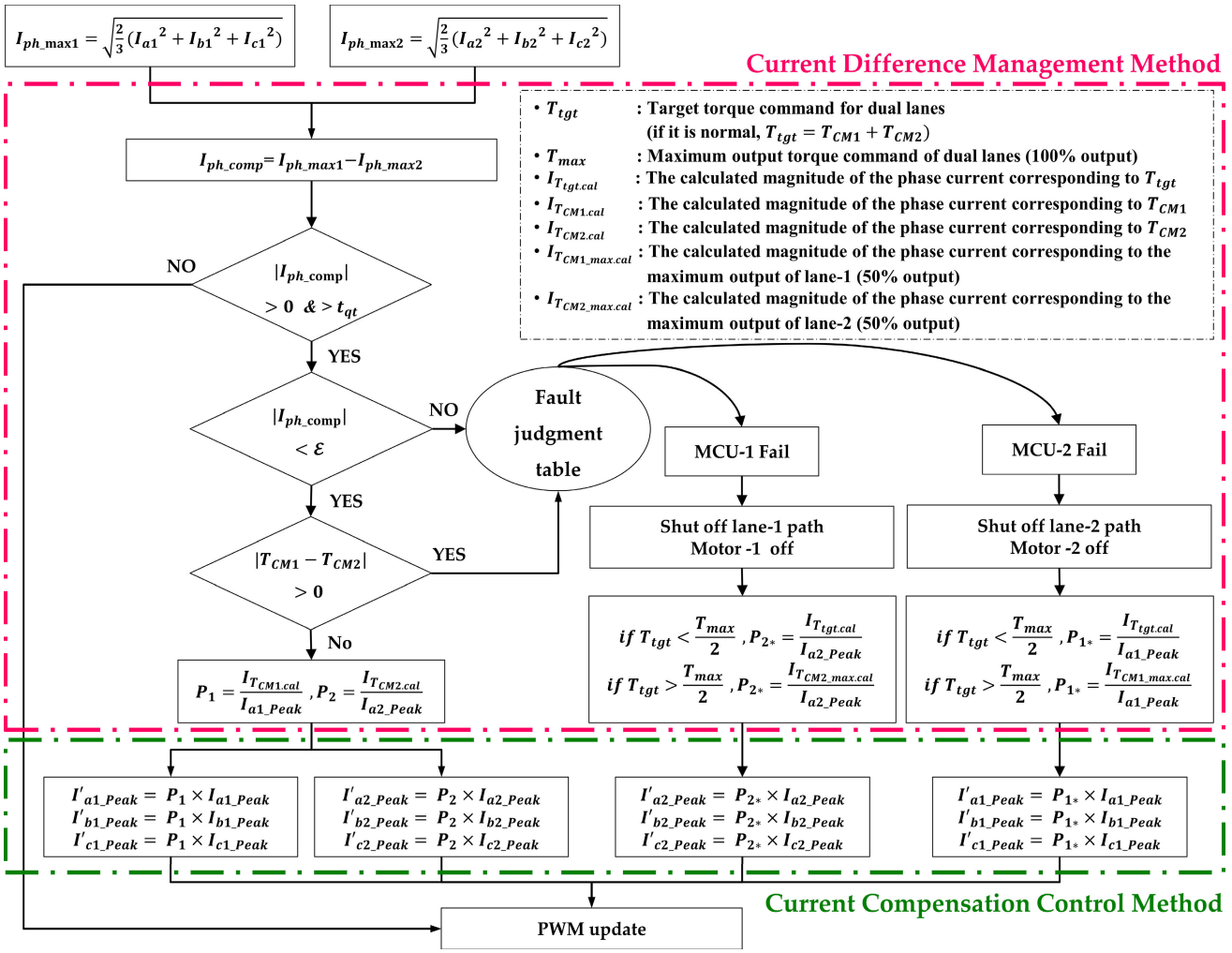

FIGURE 7. Flowchart of the proposed CDMM and CCCM.

to the T_{tgt}. At this point in time, the gain is the ratio of the calculated current value corresponding to the T_{tgt}, $I_{T_{tgt.cal}}$ and the sensed peak phase current values of the normal lane, I_{pk_Peak}, $(p = a, b, c, k = 1, 2)$.

11) If the T_{tgt} is more than half of the T_{max}, the gain is adjusted by the magnitude of the current corresponding to the maximum output that the normal lane can output (50% of T_{max}). At this point in time, the gain is the ratio of the calculated current values corresponding to the maximum output of the normal lane, $I_{T_{CMk\_max.cal}}$, $(k = 1, 2)$ and the sensed peak phase current values of the normal lane, I_{pk_Peak}, $(p = a, b, c, k = 1, 2)$. The reason for limiting the current increase is to avoid failure of even the normal lane by exceeding the current capability limit. By providing limited torque assist, it avoids an emergency situation, continues driving and alerts the driver at the same time.

The current control methods of the dual three-phase PMSMs have been proposed in numerous previous studies [12]–[20]. The most commonly used control strategies are the vector space decomposition control [12]–[16] and two-individual current control methods [17]–[20]. In this paper, rather than the control method of the dual three-phase PMSMs, which are already well-known, a current compensation control strategy is proposed to make the different currents the same or to increase the current of one lane for failure operation scenarios.

Details of the control method for current compensation are shown in the control functional block diagram in Fig. 8(a). The I_{ph_max1} and I_{ph_max2} values sensed from each current-sensing circuit are inputted into the CDMM block. In the normal lane, the proportional gain P is calculated according to each case described above, and the failed lane is then isolated through the shut-off path. The P gain calculated for each case compensates each phase current and the compensated phase currents are converted into the dq-axes current and fed back so that the PWM output of each gate driver IC changes. In the phase current feedback loop, proportional gain control is used to change the sensed phase currents without affecting the original motor control algorithm.

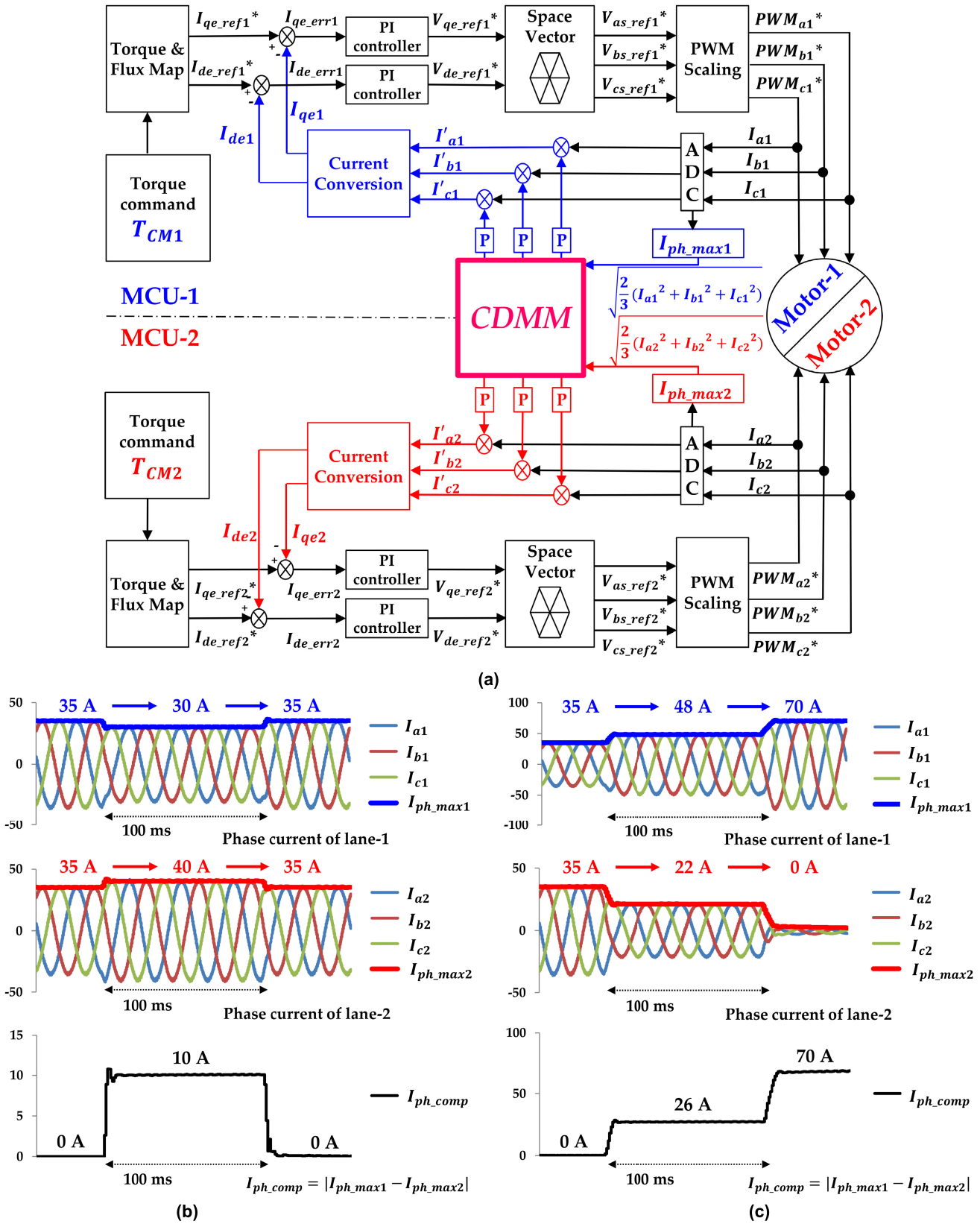

FIGURE 8. Proposed current compensation control method: (a) functional block diagram of the current compensation control in detail, (b) simulation result when the $I_{ph\_comp} < \varepsilon$ and $T_{CM1} = T_{CM2}$, (c) simulation result when the $I_{ph\_comp} > \varepsilon$.

Simulation verification for the proposed CCCM was performed as shown in Fig. 8(b) and (c). In the case of Fig. 8(b), when $T_{CM1} = T_{CM2}$ and the current difference (I_{ph_comp}) was less than the diagnostic threshold of 14 A, the two currents

were compensated and controlled so as to be the same and the difference between them became zero. The filtering time was set to 100 ms. In the case of Fig. 8(c), when the current difference was more than the diagnostic threshold of 14 A, the phase current of the failed lane-2 (assume that the MCU-2 has a failure) became zero because the gate driver IC was disabled and the current of the normal lane-1 was increased to the magnitude of phase current 70 A, which was capable of producing the target torque 2.7 Nm required to recover the torque assist function (2.7 Nm corresponds to 50% of T_{max} in dual lanes). The electrical phases of the phase currents of each lane were kept the same during the simulation process. This proposed CCCM can compensate for the imbalance between the phase currents of motors −1 and −2 in order to improve the performance of the torque and efficiency and serves as a powerful safety measure that maintains failure operation by increasing the output of the one normal lane in case of emergencies.

V. EXPERIMENTAL VERIFICATION

A. PROTOTYPE OF THE DW-PMSMS AND DUAL ECUS AND TEST SET-UP

A prototype of the DW-PMSMs was fabricated in the dual three-phase with an 8-pole, 12-slot combination, as is shown in Fig. 9(a). The length and diameter of the stator core were 67 mm and 88 mm, respectively, and the maximum phase current of each motor was 70 A. The dual ECUs were designed on one board (FR-4, 8-Layers), with ECUs −1 and −2 fully electrically-isolated, as is shown in Fig. 9(b).

The voltage supply lines (BAT-1, BAT-2), two three-phase output power lines (A1, B1, C1/ A2, B2, C2) and ground lines (GND-1, GND-2) were completely isolated between ECUs −1 and −2. Each ECU board featured a main MCU, an aux MCU, a gate driver IC and power-switching MOSFETs in the three-phase bridge. Three shunt resistors for each ECU were also used as the current sensors in order to measure the motor current. The ECUs −1 and −2 could control each three-phase motor. The arithmetic operation of each MCU and the phase currents of each motor between the dual lanes could be monitored through CAN communication between the two ECUs.

The test bench was set up as shown in Fig. 9(c) and consisted of two programmable power sources, dual ECUs, DW-PMSMs, torque and speed sensors, dynamometer, oscilloscope, load controller and a control PC. Each voltage supply of the dual ECUs was 14 V and these supplies were separated using two programmable power sources. The rotary position sensor board was mounted on the sensing magnet of the DW-PMSMs

B. RESULTING TORQUE AND EFFICIENCY OF THE DW-PMSMS ACCORDING TO THE CURRENT RATIOS

In order to measure the combined torque and efficiency, the ratios of the phase currents of each motor were experimentally-controlled by applying the current command. The current through each winding was varied from 0 A to 70 A in increments of 7 A. The phase current of each winding

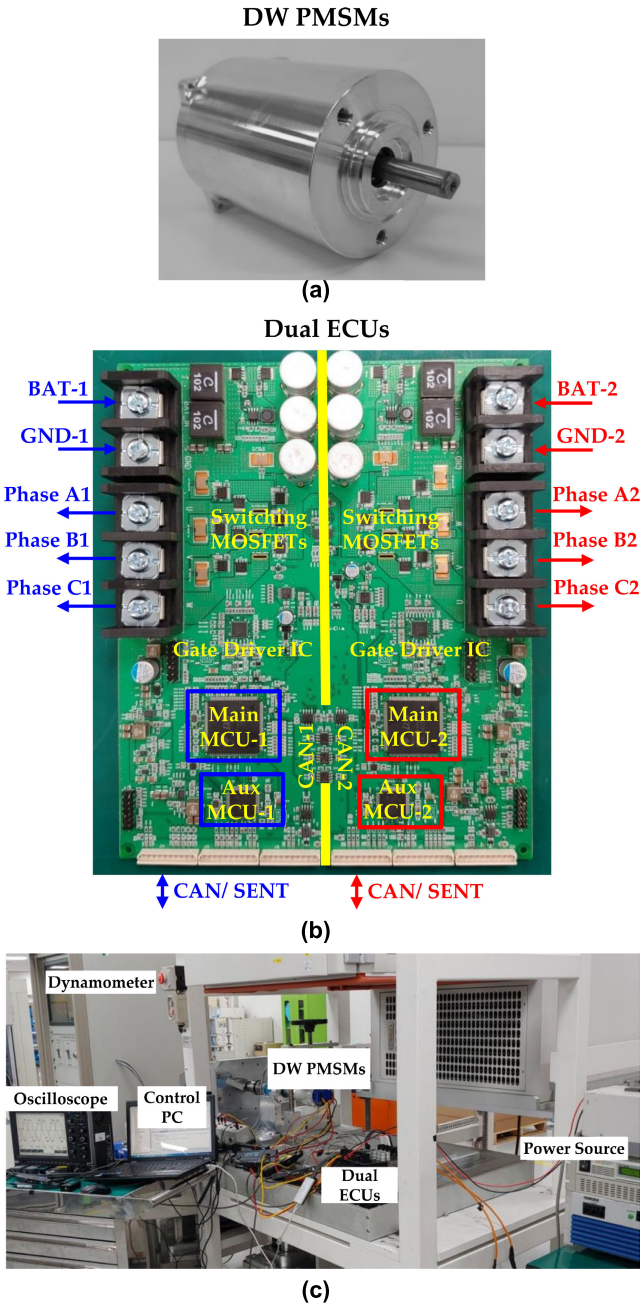

FIGURE 9. Prototype of: (a) DW-PMSMs, (b) dual ECUs, and (c) the test bench.

was monitored using an oscilloscope. The sum of the torque and efficiency were measured at 1000 rpm as a function of the ratios of each of the currents. In order to minimise the side effects of motor deterioration due to continuous operation, the measurements were performed with an adequate time-gap based on the experimental case of the current ratios. The torque was measured over a period of 6 s. The measurement results are summarised in Table 4.

The changes in the measured torque and efficiency were plotted as shown in Fig. 10(a) and (b). In Fig. 10(a), the combined torque tends to decrease, as the difference between

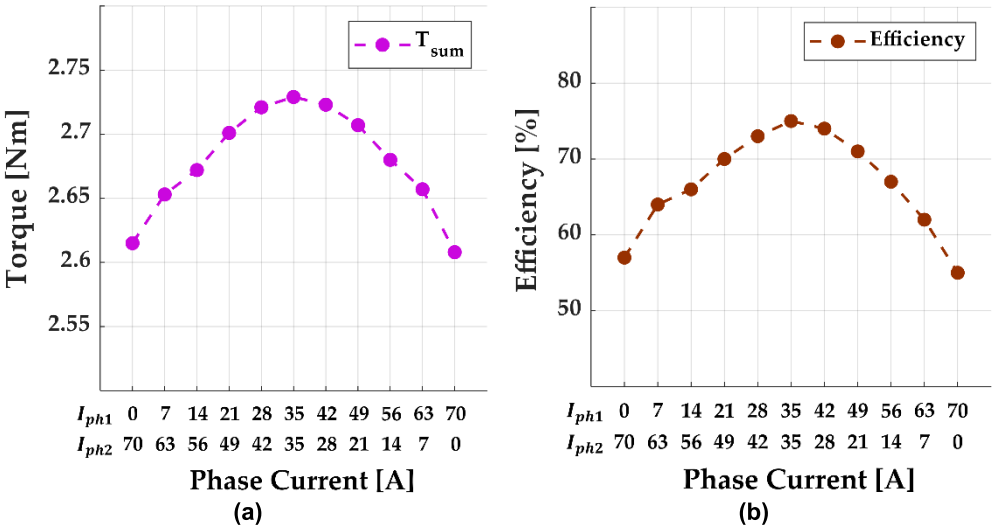

FIGURE 10. Measured changes in: (a) the torque of the DW-PMSMs, and (b) the efficiency of the DW-PMSMs.

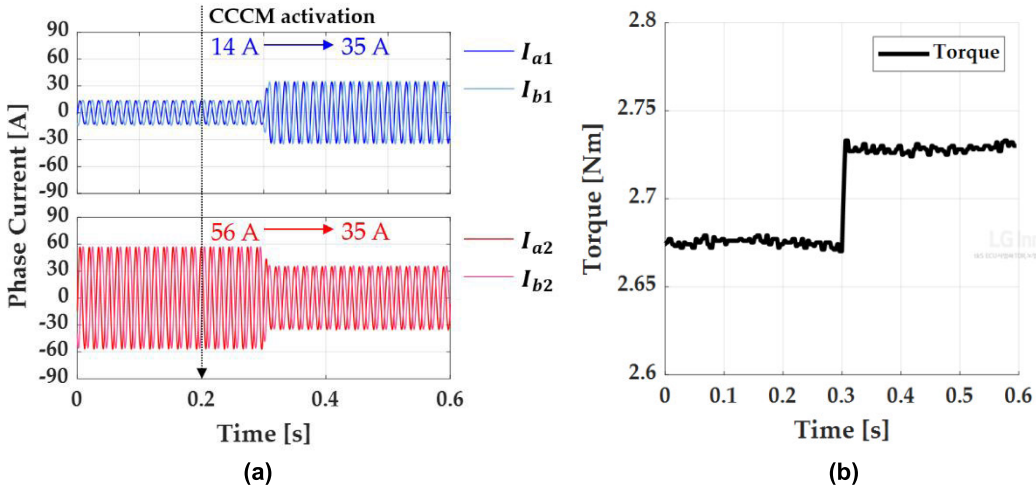

FIGURE 11. Measured changes: (a) of the phase current of the DW-PMSMs, and (b) in the torque of the DW-PMSMs.

TABLE 4. Measurement result of the torque, loss and efficiency of the DW-PMSMs at $\omega = 1000$ rpm.

I_{ph1} [A]	I_{ph2} [A]	P_{in} [W]	T_{sum} [NM]	P_{out} [W]	P_{loss} [W]	η [%]
0	70	477	2.615	274	203	57.4
7	63	433	2.653	278	155	64.1
14	56	421	2.672	280	141	66.5
21	49	401	2.701	283	118	70.4
28	42	388	2.721	285	103	73.3
35	35	379	2.729	286	93	75.3
42	28	384	2.723	285	99	74.2
49	21	396	2.707	283	113	71.5
56	14	419	2.680	281	138	67.0
63	7	450	2.657	278	172	61.7
70	0	499	2.608	273	226	54.7

the currents flowing through each of the windings increases. The combined torque is the highest when the current ratios are equal. For the current ratio of 70 A:0 A, the combined torque decreased by 4.4% compared to the current ratio of 35 A:35 A. Because the electrical phases of the currents flowing through each of the windings are equal, there was little difference in the torque ripple, as per the change in the current ratios. Moreover, in Fig. 10(b), the efficiency of the measured DW-PMSMs exhibits a similar trend. The efficiency is highest when there is no current imbalance, and the greater the current imbalance, the lower the efficiency. Changes in both the measured torque and efficiency of the DW-PMSMs are very similar to the previously-calculated and simulated changes.

When the phase currents of the DW were different and the same, the changes in the current and torque were measured. Initially, each winding was driven by a different phase current and the proposed CCCM was activated to match its magnitude. As it was to measure the current and torque change when the current difference between windings −1 and −2 disappeared, the CDMM was not applied. Because each

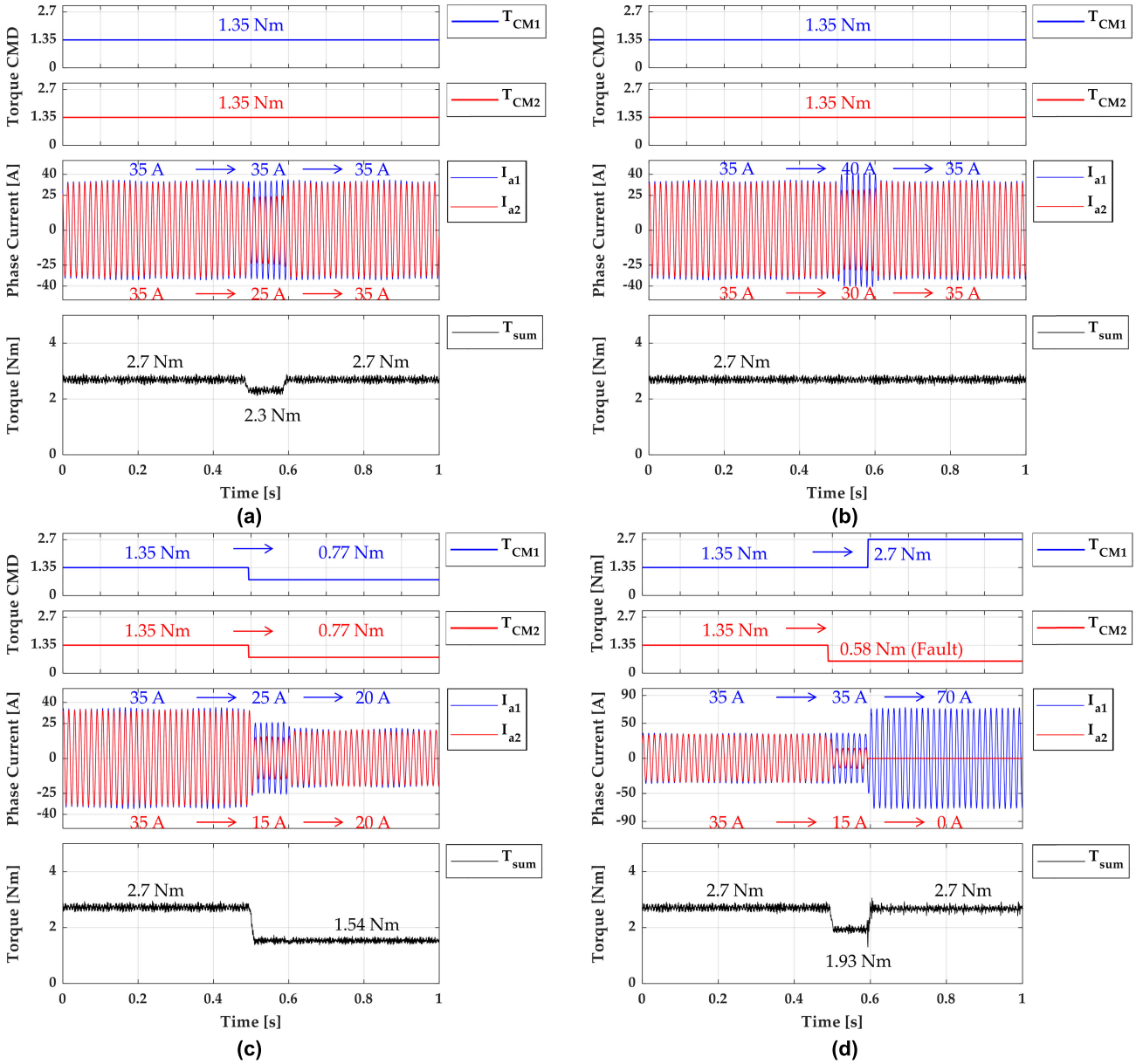

FIGURE 12. Measurement results of the torque command (T_{CM1}, T_{CM2}), phase currents (I_{a1}, I_{a2}) and combined torque (T_{sum}) change in the dual lanes: (a) $\varepsilon < 14$ A, $T_{CM1} = T_{CM2}$, no T_{tgt} change and a current deviation of only lane-2, (b) $\varepsilon < 14$ A, $T_{CM1} = T_{CM2}$, no T_{tgt} change and current deviations of both lanes, (c) $\varepsilon < 14$ A, $T_{CM1} = T_{CM2}$, T_{tgt} change and current deviations of both lanes, and (d) $\varepsilon > 14$ A and a failure of lane-2.

ECU had separate power and ground, current synchronisation, comparison and compensation between the MCUs of each ECU were achieved via CAN communication. Currents in phases A1, B1, A2, and B2 were measured. As is shown in Fig. 11(a), the currents of each motor initially differed, but they were equal after the proposed compensation algorithm was activated. Before application of the algorithm, the phase currents of motors −1 and −2 were maintained at 14 A and 56 A, respectively, and after the application of the compensation algorithm, with 100 ms interval, each phase current changed to 35 A. As was previously verified, as the phase current difference between the motors disappeared, the average torque increased by approximately 2%, from 2.675 Nm to 2.728 Nm, as is shown in Fig. 11(b). As the current was automatically compensated for, the combined torque increased as well. In other words, it was proven that the DW-PMSMs had the maximum efficiency and torque performance when the phase currents of each winding were the same.

C. VERIFICATION OF THE PROPOSED CDMM AND CCCM

In order to verify failure detection and reaction in dual lanes to which the CDMM and CCCM were applied, the fault-injection test was used to differentiate the torque commands or phase currents between the two lanes. Several methods of fault-injection testing can be utilised for safety testing [21]–[24]. During runtime, a runtime injection method

was utilised to create a torque command difference or current difference using a software trigger. A manipulation layer replaced the actual raw data with virtual fault data to be injected, which could be selected and monitored in the MCU. The fault was then injected through the XCP on CAN.

When the current difference was less than 14 A, it was noted that the difference in the two currents was detected as a deviation rather than a failure and the recovery reverted to the same currents. Three test cases were measured when the torque command had not changed, but there was a current deviation in only one lane, when the torque command had not changed, but there were current deviations in both lanes, and when the torque command had changed and there were current deviations in both lanes. The total target torque of the dual lanes T_{tgt} was 2.7 Nm (the target torque of each lane was 1.35 Nm) and the changed target torque T_{tgt} was 1.54 Nm (the target torque of each lane was 0.77 Nm). The change in the phase current and torque of each lane at 1000 rpm was measured in accordance with the test cases.

The measurement graphs of the phase current and torque change when a current deviation occurred in only one lane and the torque command values of the two MCUs were kept the same are shown in Fig. 12(a). The phase currents of both lanes were initially operated equally at 35 A and, following the current deviation fault injection, the phase current of lane-2 was reduced to 25 A. With a time interval of 100 ms, the current of lane-2 was compensated for and the phase currents of both lanes were recovered equally, to 35 A. The change in the average combined torque decreased to 2.3 Nm when the currents in the two lanes differed and then equally recovered to 2.7 Nm again.

The measurement graphs of the phase current and torque change when the current deviations occurred in both lanes and the torque command values of the two MCUs were kept the same are shown in Fig. 12(b). The phase currents of both lanes were initially operated equally at 35 A and, after the current deviation fault injection, the phase current of lane-1 was increased to 40 A and that of lane-2 was decreased to 30 A. The currents of both lanes were also recovered equally to 35 A with a time interval of 100 ms. The change in the average combined torque did not noticeably change whether or not there was a current difference. The reason is that the sum of the two currents was the same and the difference between the two currents was not as large as 10 A.

The measurement graphs of the phase current and torque change when the current deviations occurred in both lanes and the torque command values of the two MCUs were changed are shown in Fig. 12(c). The phase currents of both lanes were initially operated at 35 A and the current deviation faults were injected so that the currents incorrectly changed when T_{CM1} and T_{CM2} were changed. When the target torque command T_{tgt} was changed from 2.7 Nm to 1.54 Nm, the phase current of lane-1 was incorrectly controlled to 25 A and the phase current of lane-2 to 15 A and then, both currents were equally controlled to 20 A according to the changed torque command, with a time interval of 100 ms.

Finally, when the current difference was greater than 14 A, the failure detection and fail-operational functions were tested. In order to isolate the failed lane, the PWM output of the gate driver IC of faulty lane-2 was turned off. As is shown in Fig. 12(d), when the total target torque of the dual lanes was 2.7 Nm (the target torque of one lane was 1.35 Nm), both lanes had the same phase current output of 35 A. At this time, the fault torque command value 0.58 Nm corresponding to phase current 15 A was injected into MCU-2. After 100 ms, the phase current in lane-2 became zero and the phase current in lane-1 increased to the maximum phase current value of 70 A. Like the torque change graph shown in Fig. 12(d), even if lane-2 was disabled, it could be confirmed that failure operation or torque assist was possible by increasing the torque for lane-1.

VI. CONCLUSION

In this study, the current ratios of redundant systems consisting of DW-PMSMs with symmetrical mounted windings and dual ECUs were investigated. The optimal current ratio of the dual lanes for the torque and efficiency of the DW-PMSMs were derived and analysed. As a result, it was demonstrated that there was an optimal performance at the same current ratio and that it was highly important that the currents were balanced, not only to minimise loss but also to avoid unbalanced rotational magnetic fields. And, when the currents were not controlled equally, as intended, a diagnostic process and new diagnostic method were proposed. The optimal diagnostic threshold for determining whether or not the current difference was from a failure was selected by means of a worst-case analysis. And, the fault judgment table that can distinguish which lane was true when a disagreement occurred in the dual lanes was proposed. With the previously selected diagnostic threshold and the proposed fault judgment table, the CDMM was proposed, which constitutes the overall diagnostic process for the current difference. In addition, the CCCM was proposed to change the current so as to match the same or increase the current of the normal lane in the case of failure operation. The proposed CDMM and CCCM were also experimentally-verified.

The diagnostic strategies described and verified in this paper can provide a robust safety mechanism for diagnosing each other between dual systems through monitoring and comparing the calculated torque command and output current of each lane and can resolve situations such as ''byzantine-fault'' or ''tie-breaking'', which are the biggest drawback of dual-redundant systems. These proven solutions could be applied to diverse fail-operational EPS systems equipped with dual lanes. The next phase of research on functional safety solutions for autonomous driving that is suitable for level 5 defined in SAE should therefore be continued.

REFERENCES

[1] X. Ji, J. Ge, and H. Tian, ''Reliability improvement of electric power steering system based on ISO 26262,'' in *Proc. Int. Conf. Qual., Rel., Risk, Maintenance, Saf. Eng. (QR2MSE)*, Chengdu, China, Jul. 2013, pp. 125–129.

[2] H. Kwon, R. Itabashi-Campbell, and K. McLaughlin, "ISO26262 application to electric steering development with a focus on hazard analysis," in *Proc. IEEE Int. Syst. Conf. (SysCon)*, Orlando, FL, USA, Apr. 2013, pp. 655–661.
[3] W. Zhao, M. Cheng, W. Hua, H. Jia, and R. Cao, "Back-EMF harmonic analysis and fault-tolerant control of flux-switching permanent-magnet machine with redundancy," *IEEE Trans. Ind. Electron.*, vol. 58, no. 5, pp. 1926–1935, May 2011.
[4] J. W. Bennett, G. J. Atkinson, B. C. Mecrow, and D. J. Atkinson, "Fault-tolerant design considerations and control strategies for aerospace drives," *IEEE Trans. Ind. Electron.*, vol. 59, no. 5, pp. 2049–2058, May 2012.
[5] M. Hiramine, Y. Hayashi, and T. Suzuki, "2-drive motor control unit for electric power steering," *SAE Int. J. Passenger Cars-Electron. Electr. Syst.*, vol. 10, no. 2, pp. 337–344, Mar. 2017.
[6] X. Jiang, W. Huang, R. Cao, Z. Hao, and W. Jiang, "Electric drive system of dual-winding fault-tolerant permanent-magnet motor for aerospace applications," *IEEE Trans. Ind. Electron.*, vol. 62, no. 12, pp. 7322–7330, Dec. 2015.
[7] M. Korkosz, P. Bogusz, J. Prokop, B. Pakla, and G. Podskarbi, "Comparative analysis of fault-tolerant dual-channel BLDC and SR motors," *Energies*, vol. 12, no. 13, p. 2489, Jun. 2019.
[8] B. Basler, T. Greiner, and P. Heidrich, "Fault-tolerant strategies for double three-phase PMSM used in electronic power steering systems," in *Proc. IEEE Transp. Electrific. Conf. Expo (ITEC)*, Dearborn, MI, USA, Jun. 2015, pp. 1–6.
[9] M. Barcaro, N. Bianchi, and F. Magnussen, "Analysis and tests of a dual three-phase 12-slot 10-pole permanent-magnet motor," *IEEE Trans. Ind. Appl.*, vol. 46, no. 6, pp. 2355–2362, Nov. 2010.
[10] Y. Demir and M. Aydin, "A novel dual three-phase permanent magnet synchronous motor with asymmetric stator winding," *IEEE Trans. Magn.*, vol. 52, no. 7, Jul. 2016, Art. no. 8105005.
[11] K. Yamazaki, "Torque and efficiency calculation of an interior permanent magnet motor considering harmonic iron losses of both the stator and rotor," *IEEE Trans. Magn.*, vol. 39, no. 3, pp. 1460–1463, May 2003.
[12] Y. Hu, Z. Q. Zhu, and M. Odavic, "Comparison of two-individual current control and vector space decomposition control for dual three-phase PMSM," *IEEE Trans. Ind. Appl.*, vol. 53, no. 5, pp. 4483–4492, Sep. 2017.
[13] Y. Zhao and T. A. Lipo, "Space vector PWM control of dual three-phase induction machine using vector space decomposition," *IEEE Trans. Ind. Appl.*, vol. 31, no. 5, pp. 1100–1109, Sep./Oct. 1995.
[14] H. S. Che, E. Levi, M. Jones, W.-P. Hew, and N. A. Rahim, "Current control methods for an asymmetrical six-phase induction motor drive," *IEEE Trans. Power Electron.*, vol. 29, no. 1, pp. 407–417, Jan. 2014.
[15] R. Bojoi, F. Farina, M. Lazzari, F. Profumo, and A. Tenconi, "Analysis of the asymmetrical operation of dual three-phase induction machines," in *Proc. IEEE Int. Electric Mach. Drives Conf. (IEMDC)*, Jun. 2003, pp. 429–435.
[16] R. Bojoi, E. Levi, F. Farina, A. Tenconi, and F. Profumo, "Dual three-phase induction motor drive with digital current control in the stationary reference frame," *IEE Proc.-Electr. Power Appl.*, vol. 153, no. 1, pp. 129–139, Jan. 2006.
[17] J. Karttunen, S. Kallio, P. Peltoniemi, P. Silventoinen, and O. Pyrhonen, "Dual three-phase permanent magnet synchronous machine supplied by two independent voltage source inverters," in *Proc. Int. Symp. Power Electron. Power Electron., Electr. Drives, Autom. Motion*, Sorrento, Italy, Jun. 2012, pp. 741–747.
[18] G. K. Singh, K. Nam, and S. K. Lim, "A simple indirect field-oriented control scheme for multiphase induction machine," *IEEE Trans. Ind. Electron.*, vol. 52, no. 4, pp. 1177–1184, Aug. 2005.
[19] R. Bojoi, M. Lazzari, F. Profumo, and A. Tenconi, "Digital field-oriented control for dual three-phase induction motor drives," *IEEE Trans. Ind. Appl.*, vol. 39, no. 3, pp. 752–760, May 2003.
[20] Y. He, Y. Wang, J. Wu, Y. Feng, and J. Liu, "A simple current sharing scheme for dual three-phase permanent-magnet synchronous motor drives," in *Proc. 25th Annu. IEEE Appl. Power Electron. Conf. Expo. (APEC)*, Palm Springs, CA, USA, Feb. 2010, pp. 1093–1096.
[21] M. Kooli and G. Di Natale, "A survey on simulation-based fault injection tools for complex systems," in *Proc. 9th IEEE Int. Conf. Design Technol. Integr. Syst. Nanosc. Era (DTIS)*, Santorini, Greece, May 2014, pp. 1–6.
[22] C. Yang, C. Yang, T. Peng, X. Yang, and W. Gui, "A fault-injection strategy for traction drive control systems," *IEEE Trans. Ind. Electron.*, vol. 64, no. 7, pp. 5719–5727, Jul. 2017.
[23] W. Bin, M. Kai, H. Xin, R. Shan, W. Fang, and S. Haotian, "Fault injection test for MCU based on E-motor emulator*," in *Proc. 2nd Int. Conf. Inf. Syst. Comput. Aided Educ. (ICISCAE)*, Dalian, China, Sep. 2019, pp. 267–269.
[24] C. Sasikumar, R. Agrawal, S. Gupta, S. Gupta, and R. Maheshwari, "Built in self-test for fault tolerant real time in-vehicle networks through automotive diagnostics," in *Proc. Int. Conf. Emerg. Trends Netw. Comput. Commun. (ETNCC)*, Udaipur, India, Apr. 2011, pp. 379–382.

YOUNGWOO NOH received the M.S. degree in electrical and computer engineering from Seoul National University, Seoul, South Korea, in 2005. He is currently pursuing the Ph.D. degree with the Department of Electrical Engineering, Hanyang University, Seoul, South Korea. Since 2005, he has been researching in an automotive motor drive engineering and is currently working as a professional engineer at LG IT Research and Development center. His research interests include electric motor control, power electronics, automotive electronic controller design, fault-tolerant design, functional safety design, and hybrid electric vehicles.

WONKYU KIM received the M.S. degree in electrical engineering from Hanbat University, Deajeon, South Korea, in 2011. He is currently pursuing the Ph.D. degree with the Department of Electrical Engineering, Hanyang University, Seoul, South Korea. Since 2011, he has been researching in an automotive motor drive engineering and is currently working as a Senior Engineer at the LG IT Research and Development Center. His research interests include electric motor control, power electronics, automotive electronic controller design, automotive sensor design, and hybrid electric vehicles.

JU LEE (Senior Member, IEEE) received the M.S. degree from Hanyang University, Seoul, South Korea, in 1988, and the Ph.D. degree in electrical engineering from Kyusyu University, Japan, in 1997. He joined Hanyang Univeristy, in 1997, where he is currently a Professor with the Department of Electrical and Bio-Engineering. His main research interests include electric machinery and its drives, electro-magnetic field analysis, transportation systems, such as hybrid electric vehicles and railway propulsion systems. He is a member of the IEEE Industry Applications Society, the Magnetics Society, and the Power Electronics Society.